Experimental investigation of disruptive burning phenomena on nanofuel droplets

Inês A. S. Ferrão[1,2,3*], Miguel A. A. Mendes[1], Ana. S. O. H. Moita[2,4], André R. R. Silva[3]

1: IDMEC-LAETA, Instituto Superior Técnico, Universidade de Lisboa, Lisboa, Portugal
2: IN$^+$-LARSyS, Instituto Superior Técnico, Universidade de Lisboa, Lisboa, Portugal
3: AEROG-LAETA, Universidade da Beira Interior, Covilhã, Portuga
4: CINAMIL, Portuguese Military Academy, Lisboa, Portugal
*Corresponding author: ines.ferrao@ubi.pt

Keywords: Nanoparticles, puffing, micro-explosion, single droplet combustion, image acquisition.

ABSTRACT

The transport sector plays a crucial aspect in society and economic evolution. However, improper energy management has negatively impacted health and the environment. Thus, the use of sustainable and green fuels in the aeronautical industry has been implemented due to environmental concerns and the depletion of fossil fuels. The introduction of biofuels, a renewable energy source in the transportation sector, has shown advantages in terms of pollutant reduction. Recently, the addition of nanoparticles in the combustion of biofuel has been studied with the purpose of enhancing its combustion characteristics. Consequently, the present work evaluates nanofuel single droplet in a falling droplet method. In this way, the fiber suspension effect was neglected, and droplets in a size of 250 μm were evaluated. To this end, a comparison between pure biofuel and a nanofuel at two furnace temperatures (T = 800 ºC and T = 1000 ºC) was performed. The results reveal that disruptive burning phenomena occur when aluminum nanoparticles are added to the biofuel. Consequently, a micro-explosion determines the end of the droplet lifetime, mainly affected by the furnace temperature.

1. Introduction

Experimental studies on liquid fuel evaporation and combustion have been intensively conducted in the past decades. These investigations aim to acquire a fundamental understanding of spray combustion. In the transportation field, spray combustion is a source of energy for compression ignition engines and aviation, marine, or land-based gas turbines, being a complicated combination of multi-scale and multi-physics phenomena. Due to its complexity, an approach to better understand the spray combustion performance and underlying mechanisms is the study of single droplet evaporation/combustion (Li et al. (2020); Z. Wang et al. (2022)). Different techniques have been developed to evaluate single droplet evaporation/combustion in terms of droplet size evolution and flame structure. In this context, four methods can be encountered in the literature:

suspended droplet, free-falling droplet, levitated droplet, and porous sphere. Figure 1 shows the most common experimental approaches used to evaluate single droplet evaporation/combustion. The advantages and disadvantages can be identified depending on the experiment purpose based on the study objective and the employed technique. Z. Wang et al. (2022) reported the recent progress observed in the experimental investigations on fuel droplet evaporation. In addition, the authors described the advantages and limitations of the majority of experimental setups displayed in Figure 1. The droplet suspended technique is mainly used for its simplicity in measuring the droplet parameters. However, using a supportive fiber does not allow the study of a relatively small droplet. The typical droplet diameters in this experimental setup are around 1mm, which is considerably higher than droplets produced by liquid fuel atomization. Moreover, the thermal conductivity of the supportive fiber influences the burning rate and disruptive burning phenomena as reported by Basu & Miglani (2016) and J. Wang et al. (2020).

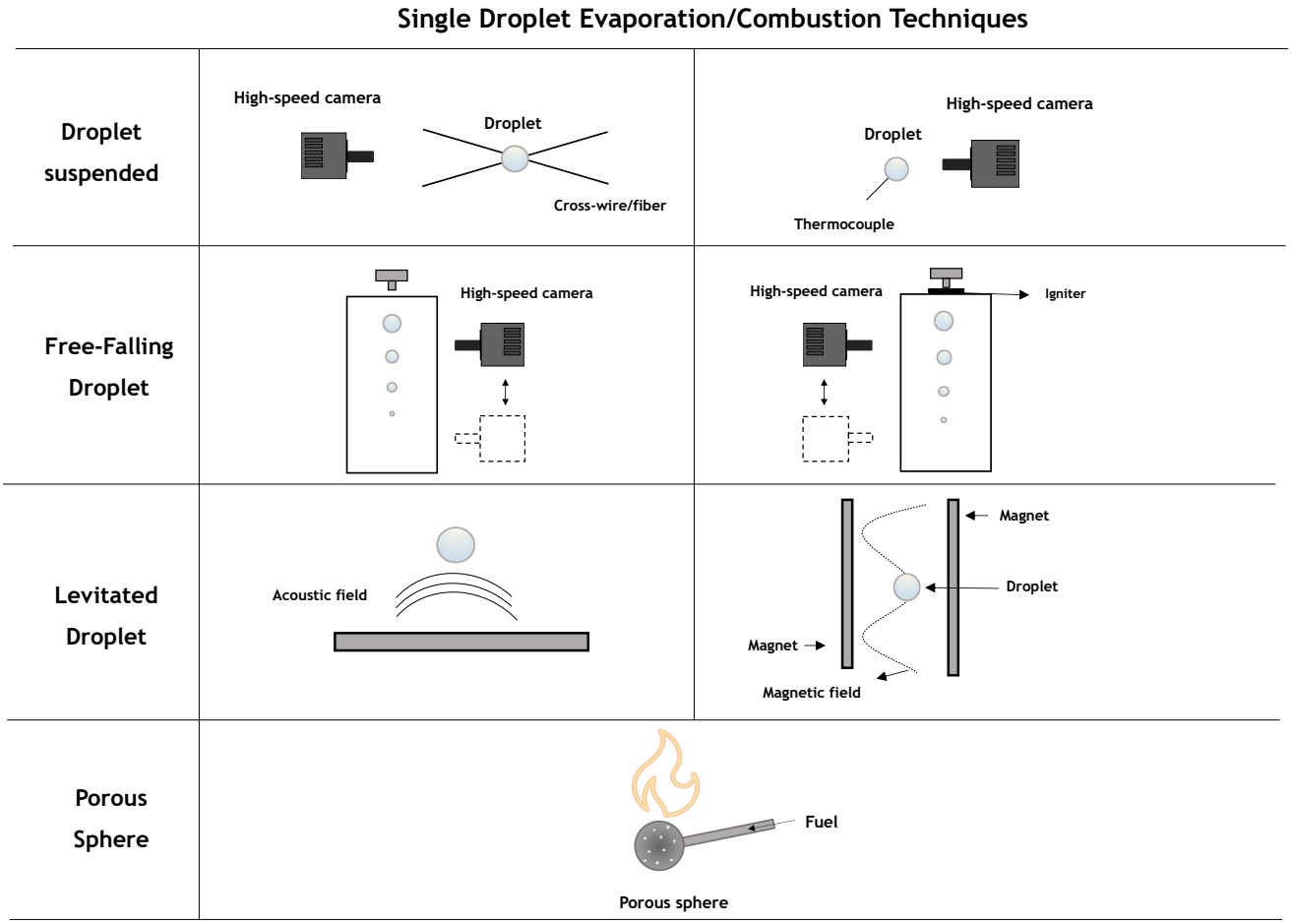

Figure 1. Illustration of experimental techniques used to study the evaporation and combustion of single droplets.

In contrast with the droplet suspended, the free-falling droplet method allows the study of droplets on a micrometer scale, and no foreign elements/filaments are presented in the experimental arrangement. In this respect, the droplet enters the combustion chamber and can achieve, in some cases, higher temperatures and pressures to recreate the operating conditions of practical engines (Chung & Kawaguchi (1990)). However, regarding the limitations of this experimental method,

Z. Wang et al. (2022) reported that the measurement of droplet characteristics is difficult due to droplet motion, being the process of tracking more complex. In addition, the droplet-air interaction affects the evaporation/combustion since the droplet is presented in a convective environment. In the levitated droplet method, the droplet parameters are easy to acquire, and there is no influence of fiber or thermocouples. Nevertheless, it is not suitable for higher ambient temperatures. Brenn et al. (2007) evaluated experimentally with the acoustic levitator the evaporation of multicomponent droplets. The experimental results were further compared with a theoretical model, and a good agreement was reported. The porous spheres are used to examine the flame insights as studied by Parag & Raghavan (2009). This technique consists of injecting the liquid fuel into the porous sphere, which can be relatively large and difficult to recreate the spray conditions. Regardless of the experimental technique used, to fully capture with detail the evaporation/combustion characteristics, an high-speed or IR camera is required, as noticed in several studies of Singh et al. (2019); Sim et al. (2018); Yadav et al. (2021).

As previously mentioned, single droplet evaporation and combustion studies remain relevant to the comprehension of spray combustion required in real engines. Many practical combustion systems are fuelled by fossil fuels, a finite energy source responsible for greenhouse and pollutant emissions (Prakash & Davies (2020)). However, countless efforts through the scientific community or politicians to switch the negative paradigm that our world is currently facing have been performed. Thus, the aviation sector, one of the largest transportation industries, has investigated and introduced alternative jet fuels with the purpose of using sustainable and green fuels. Based on this, Hari et al. (2015) evaluated the opportunities and challenges in developing alternative fuels for aviation. According to the authors, hydroprocessed renewable jet fuel and Fisher-Tropsch fuels are the most favorable fuels to replace conventional jet fuels. A more detailed description of the biofuel production technologies suitable for aviation can be found in Ferrão et al. (2021) and Doliente et al. (2020). To evaluate the introduction of alternative jet fuel, several experimental investigations focused on the combustion of jet fuel and biofuels have been performed. Muelas et al. (2017) studied freely-falling droplets of butanol, Jet-A, and their mixtures in a combustion chamber capable of varying temperature and oxygen concentration. The results reveal that the evolution of droplet diameter for butanol, Jet-A, and their blends are very similar, regardless of the noticeable compositional differences. In addition, micro-explosions and soot shells were spotted. Liu et al. (2013) performed an experimental work to compare liquid fuel combustion characteristics of biofuels derived from camelina and tallow with conventional aviation fuel. In this respect, spherical droplet flame configuration was used, and the results showed that biofuels and Jet-A have very similar behaviors in terms of their burning histories, burning rates, and the evolutions of the flame and soot standoff ratios. Nevertheless, biofuels have shown a much lower sooting propensity than Jet-A. Recently, Meng et al. (2021) studied the combustion and micro-explosion characteristics of mixed droplets of aviation fuel, biodiesel, and ethanol. The variation of the operating conditions, such as, temperature and oxygen concentration, allowed the study of a micro-explosion. The disruptive burning phenomena in droplet fuel mixtures have been reported by Rao et al. (2017); Pacheco et al. (2021), being a mechanism to promote efficient combustion. Additionally, puffing

and micro-explosion were also detected in the combustion of nanofuel (Basu & Miglani (2016); Jang & Kim (2022); Li et al. (2020)). In this concept, energetic or not energetic particles in a range of 1-100 nm were stably suspended in liquid fuel. Javed et al. (2014) investigated the micro-explosion phenomenon in dense concentrations of aluminum nanoparticles added to kerosene. A droplet suspended method was used to evaluate the evaporation and micro-explosions for dense concentrations. The authors stated that micro-explosions were detected when aluminum nanoparticles were added to the kerosene. The micro-explosion intensity increases with the ambient temperature and particle concentration. Ittoo et al. (2022) investigated single droplet combustion of diesel and nanofuels composed of multiwalled carbon nanotube. Micro-explosions were identified, and their intensity depended on the particle concentrations. The above studies motivated us to examine disruptive burning phenomena of nanofuels in a falling droplet method. In this way, the fiber suspension effect was neglected, and micron-sized droplets were evaluated. A comparison between pure biofuel and a nanofuel at two ambient temperatures (T = 800 ºC and T = 1000 ºC) in terms of burning rate and puffing/micro-explosions, was accomplished. In addition, a detailed visualization and comprehension of the disruptive burning phenomena were provided.

2. Experimental Approach

The biofuel used in this work is a hydrotreated vegetable oil (HVO), named NExBTL, and is typically made from vegetable oils and animal waste fats (Nylund et al. (2011)). Table 1 shows the properties of the HVO. Aluminum nanoparticles purchased from Nanografi in a size of 40 nm were stably suspended in HVO. Additionally, a particle concentration of 1.0 wt.% was considered. Aluminum is a suitable additive to hydrocarbons due to its abundance, amount of energy release, and relatively low cost (Gür (2018)).

Table 1. HVO properties adapted from Ferrão et al. (2021); Pacheco et al. (2021); Pizziol et al. (2018).

Parameter	Standard Limit	HVO
Density (kg/m^3) (at 20 °C)	771–836	780.6
Kinematic viscosity (mm^2/s) (at 25 °C)	-	4.33
Surface tension (N/m) (at 20 °C)	-	0.0265
Final boiling point (°C)	Max. 300	308
Sulfur (wt.%)	Max. 30.0	0.09
Aromatics (wt.%)	Max. 25.0 (vol.%)	0
Lower heating value (MJ/kg)	Min. 42.8	43.9
H/C ratio	-	2.18
Carbon number	-	C15–C18

Figure 2 shows a schematic of the nanofuel preparation. The preparation of nanofuels demands a methodic procedure to accomplish homogeneous, stable, long-term suspension and a low-level

of particle agglomeration (Gan & Qiao (2011)). It is essential to highlight that suspension stability is crucial in nanofuel studies. The nanoparticles were first vigorously stirred for 20 minutes with the liquid fuel. Subsequently, the nanofuel (HVO + n-Al) was sonicated in an ice bath. The sonicator (model UP200Ht by Hielscher) was used to disperse the particles and avoid agglomeration. Afterward, the nanofuels stability was evaluated in a tube test for several hours and days. It was observed that HVO + 40 nm (1.0 wt.%) lasted for 6 hours as a homogeneous solution. In this study, there was no addition of surfactant to the nanofuel.

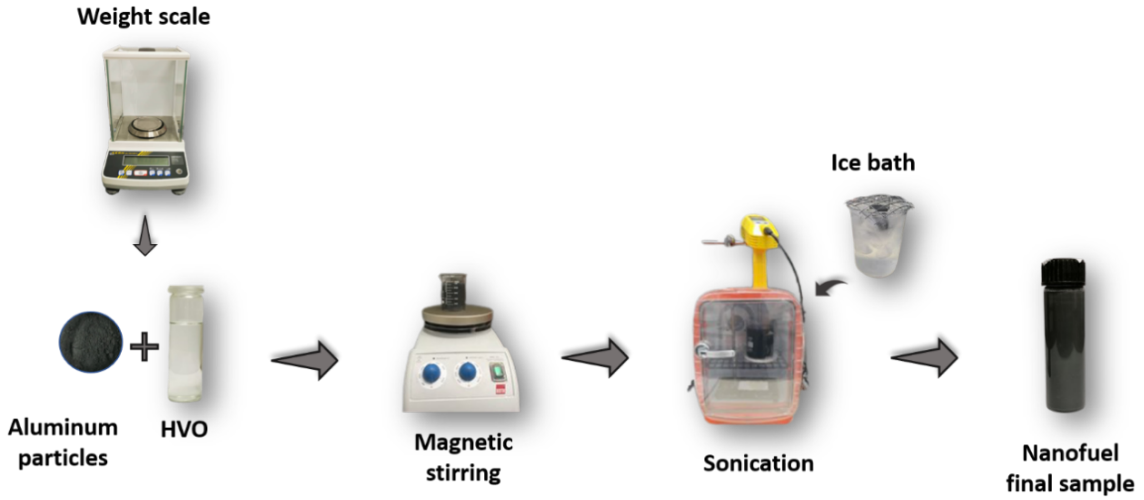

Figure 2. Nanofuel preparation procedure.

Figure 3 shows the physical properties of HVO + 40 nm (1.0 wt.%), where 3 a) corresponds to the density, 3 b) surface tension, and 3 c) viscosity. The density was measured at room temperature (20 ± 3 ºC) with Densimeter DA-130N, and surface tension was measured using the pendant drop method with an optical tensiometer THETA (Attension). Regarding the viscosity, Brookfield DV3TRVCP Rheometer was used, and its accuracy is ± 1.0% of the range. No significant alteration of the physical properties of nanofuel, compared to pure biofuel, was noticed.

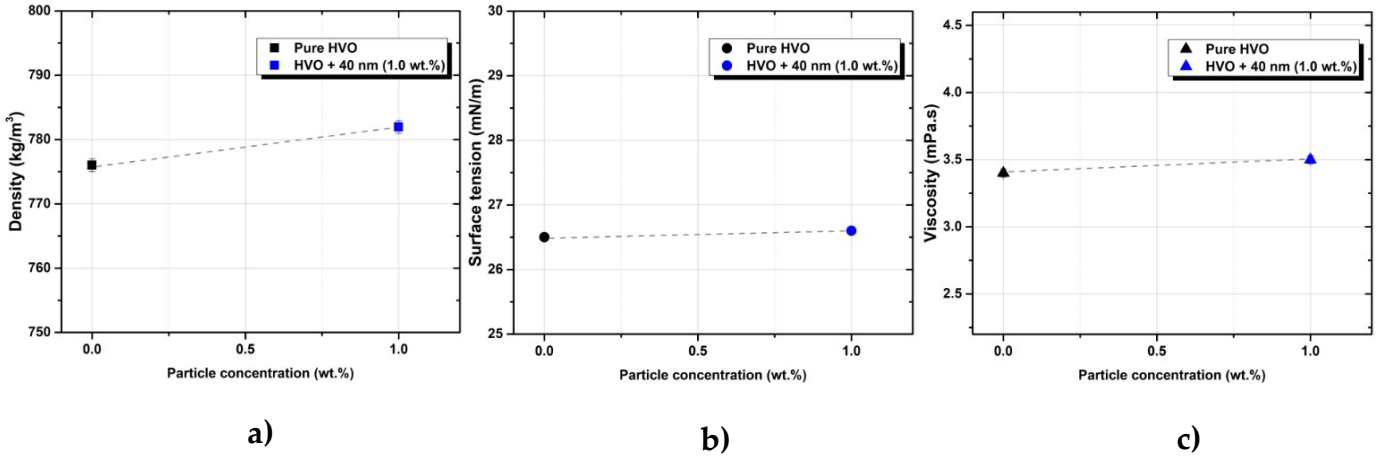

Figure 3. HVO and nanofuel properties: a) Density; b) Surface tension; c) Viscosity.

The combustion of pure biofuel and nanofuel was evaluated in a drop tube furnace. Figure 4 shows the experimental setup used in this work. This droplet combustion facility consists of an electrically heated drop tube furnace (DTF), an illumination set, an image acquisition system, and an injector device. The DTF possesses electric coils, and it is capable of varying the wall temperature and oxygen concentration. Additionally, the DTF has two opposed rectangular windows with 2 cm width and 20 cm for optical access. The single droplet combustion occurs inside the vertical quartz tube with an inner diameter of 6.6 cm and a length of 82.6 cm placed inside the DTF. The injection of droplets and air occurs in a different inlet in the DTF injector. The air supply enters at the injector with a flow rate of 5.7 L/min with a precision error of ± 2% and creates a proper environment for the droplet autoignition. Droplets were generated by a TSI device using a pinhole with 200 μm placed at the top of the DTF injector. The droplet stream is achieved using a syringe pump and frequency generator with the following operating conditions: 2.1 kHz and 1.3 mL/min flow rate. Droplets with an initial diameter of 250 μm were evaluated, and to guarantee the space/time between droplets, a rotating disk was used to ensure the analysis of single droplet combustion. The rotating disk has a rotational speed of 1200 rpm and a 1 cm x 1 cm slot that allows the droplet entrance to the quartz tube inside the DTF. The illumination set comprises a LED light and a diffusion glass to enhance the contrast for a better visualization. To follow the burning process from the injector tip until the micro-explosion, a CMOS high–speed camera (CR600×2, Optronics), coupled with a high magnification lens, was used. The magnification lens is composed of a 6.5×Zoom, 12 mm FF, a 0.25×lens attachment, and a 2.0×short adapter with a magnifying range of 0.35-2.25, leading to an increase in the spatial resolution up to 8.2 μm/pixel. The image acquisition was pursued with 1000 fps with a resolution of 1200×500 pixels and an exposure time of 1/13000 s. This experimental technique was already employed in a previous study performed by Ferrão et al. (2022). Moreover, a Photron FASTCAM mini UX50, a high-speed camera with 1.3 Megapixel, was used to acquire micro-explosions with more detail, and a high magnification lens was coupled to the camera. The high-speed camera is connected to a computer and is manually triggered. In addition, the pixel size in this study was 9 μm. The disruptive burning phenomena identified in the experimental study are difficult to acquire since its duration is brief and occurs at the end of the droplet lifetime. Furthermore, as mentioned above, the free-falling technique has a limitation on the burning tracking process. Due to this, different camera operating ranges were considered. Several frame rates of 2000, 3200, 4000, and 5000 fps and exposure times of 1/16000s and 1/20000s were used to fully capture the details of disruptive burning phenomena.

The image data processing was performed in ImageJ and MATLAB software. First, the droplet size was evaluated using ImageJ based on the droplet outline through the brightness gradient in order to obtain the burning rate. Then, the bright spots provided from the micro-explosions were identified and counted by an algorithm developed in MATLAB. As reported by Ferrão et al. (2022), to acquire the droplet size evolution during the combustion process, a region of interest (ROI) is defined. Then, the droplet outline is marked through the brightness gradient for these analyses, allowing the droplet characterization.

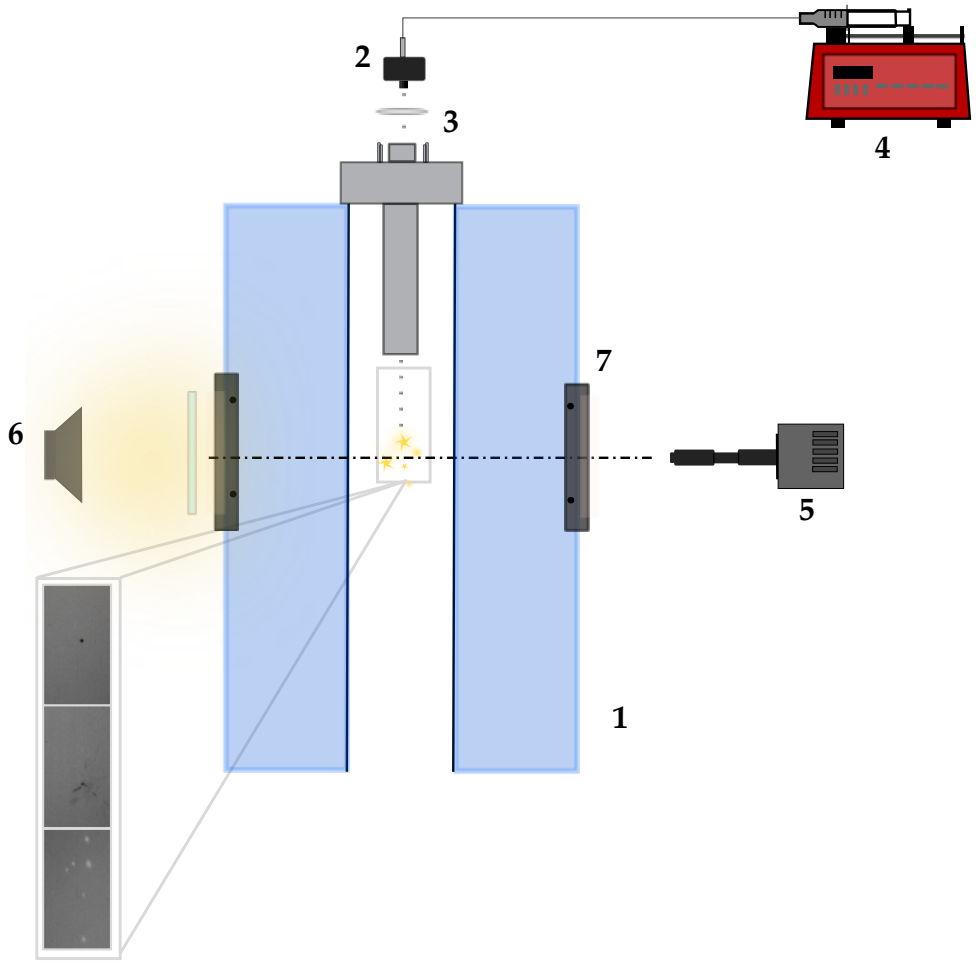

Figure 4. Experimental setup: 1 - Drop tube furnace; 2 - Commercial droplet generator; 3 - Rotating disk; 4 - Syringe pump; 5 - High-speed camera; 6 - Illumination; 7 - DTF window.

Figure 5 shows the procedure used to study the disruptive burning phenomena spotted in nanofuel. Firstly, the acquisition of images at different operating conditions was performed based on the methodology mentioned above. Subsequently, a selection and identification of micro-explosions were required to find the region of interest to be further analyzed. For each furnace temperature, 10 micro-explosions were analyzed, and more than 30 images were considered for the individual disruptive event. After this, a MATLAB algorithm was developed through subtraction, binarization, and recognizing elements in the recorded images. The background was subtracted from the micro-explosions image in order to highlight the disruptive outcomes. The following phase was image binarization using a threshold with a gradient magnitude value of 0.09. This value was considered after examining several thresholds where the cited value yielded better results. Afterward, a MATLAB function defined as *imfill* was used, and the position of the pixels with the highest value (white pixels) was detected. Finally, the algorithm returns the maximum number of fragments in the images. For this case, the elements are labeled using a *vislabels* function, and the number of fragments is given by *numel* function. The micro-explosions were divided into 4 regions of interest (ROI) to enhance the phenomena understanding. These ROIs aim to identify and count the fragments on the upper and lower sides and consider the position of the primary

droplet disruption. The location of the disruption is marked by a red circle in Figure 5.

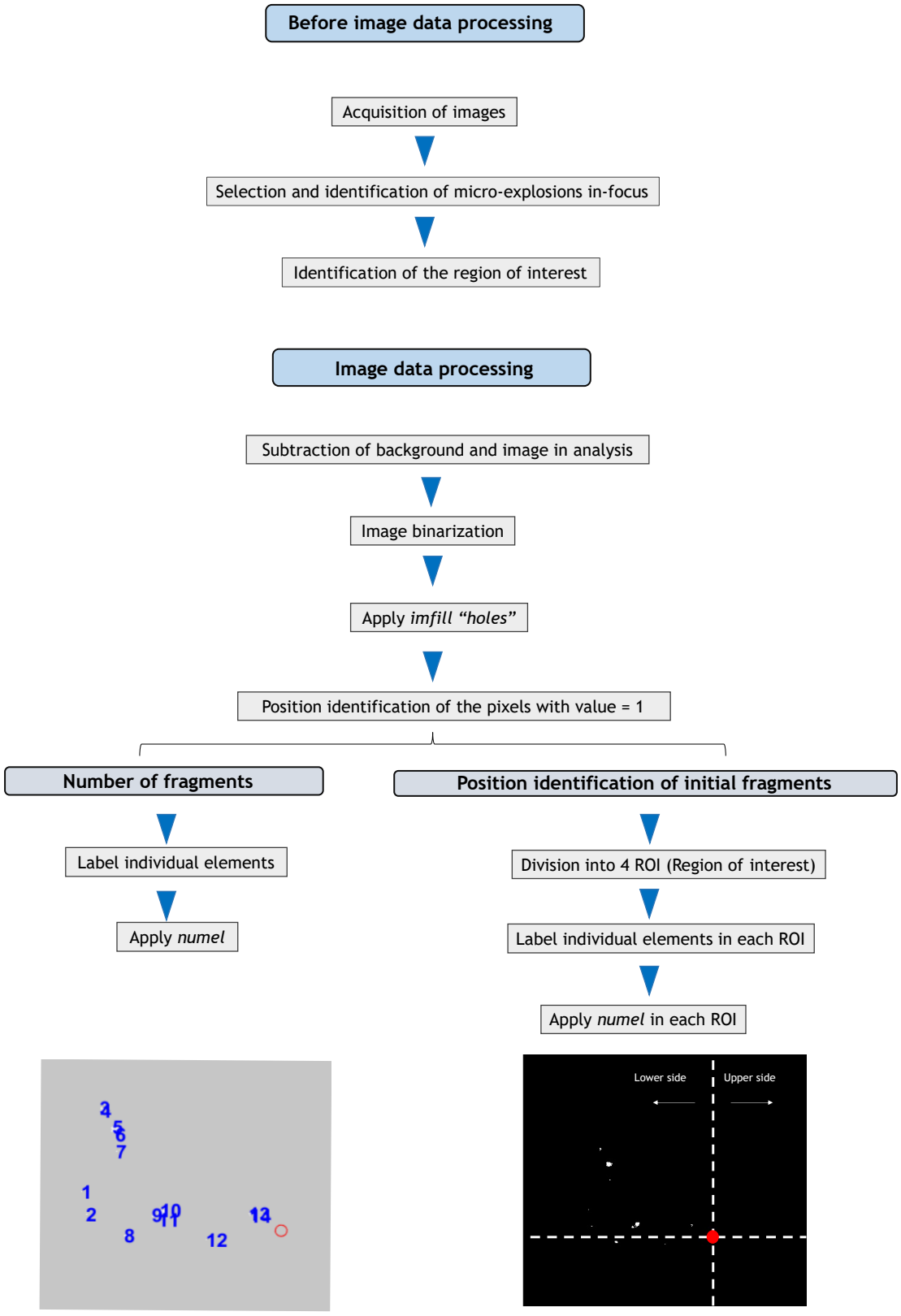

Figure 5. Image data processing.

3. Results

In the present work, a pure biofuel and nanofuel with a particle concentration of 1.0 wt.% were evaluated at two different temperatures in a drop tube furnace. Ferrão et al. (2021) and Ferrão et al. (2022) evaluated different particle sizes and concentration in a similar experimental arrangement. Consequently, the effect of adding nanoparticles to HVO in terms of droplet size evolution and burning rate has been studied. The authors mainly focused on the droplet combustion dynamics and spotted disruptive events at the end of the droplet lifetime. Regarding pure HVO combustion, puffing or micro-explosion were not detected. In this context, the burning rate was examined to understand the influence of aluminum nanoparticles in a biofuel. Figure 6 shows the burning rate for pure HVO and HVO + 40 nm (1.0 wt.%) at T = 800 °C and T = 1000 °C. According to Ferrão et al. (2022), the temporal evolution of the droplet size reduction for the pure HVO is in good agreement with D^2-law. The classical liquid droplet combustion theory states that the normalized square diameter decreases linearly with time, with a nearly constant slope, defined as the burning rate. However, when nanoparticles were added, the droplet size evolution was affected by particle aggregation and micro-explosion occurrence. Consequently, the nanofuel at T = 800 °C and T = 1000 °C does not follow the D^2-law.

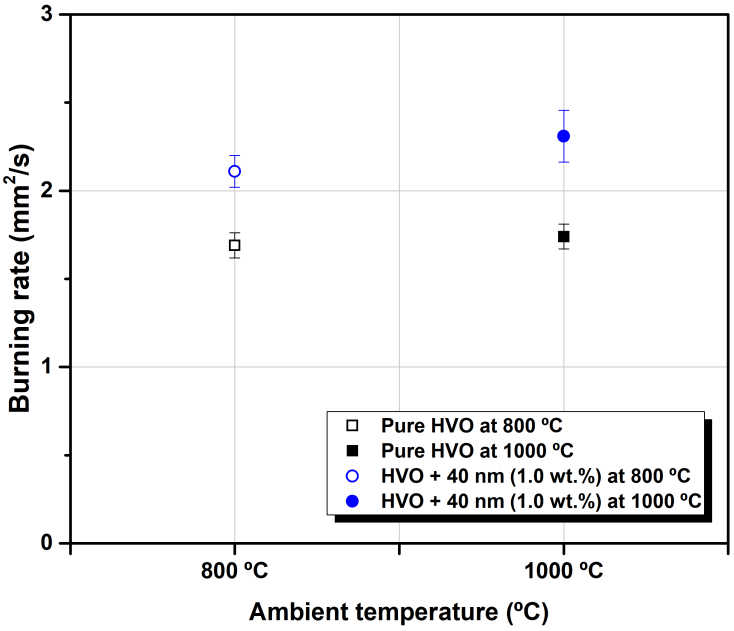

Figure 6. Burning rate for pure HVO and HVO + 40 nm (1.0 wt.%) at T = 800 °C and T = 1000 °C.

To provide comparison results, the burning rate was analyzed until t/D_0^2 = 0.35 s/mm^2, as previously mentioned by Ferrão et al. (2022). The results suggest that pure HVO presents the lowest burning rate regardless of furnace temperature. However, nanofuel displays a burning rate enhancement indicating that adding aluminum nanoparticles to a biofuel could potentially increase

the HVO combustion. According to the literature, a hypothesis for these findings is the radiation absorption, since the nanofuels are a dark and opaque fuel. The impact of nanoparticles on the combustion can be visualized at the end of the droplet lifetime due to the appearance of micro-explosions. These events promote secondary atomization, dispersing particle agglomerate and remaining liquid fuel, promoting a reduction in the droplet lifetime. A nanofuel droplet is predominantly composed of fuel, a liquid phase, and solid nanoparticles in different concentrations. Consequently, when the droplet is exposed to the high furnace temperature, the liquid phase, identified as a biofuel in the present study, evaporates. As the time proceeds, the nanoparticles stay inside the droplet and begin to accumulate at the droplet surface. Due to this, the nanoparticle concentration increases and affects the biofuel evaporation, leading to a slower reduction of the droplet diameter at the end of its lifetime. This hinders the biofuel vaporization, and as a result, the droplet surface behaves as a "shell" increasing the droplet temperature due to the energy emitted by the DTF, leading to nucleation of the liquid fuel. As a result, the pressure inside the droplet rises, ultimately prompting the shell to explode, resulting in a puffing or micro-explosion.

The disruptive burning phenomena and how they can develop in a combustion chamber are not fully understood. Thus, puffing and micro-explosions were studied on a falling droplet method to avoid interfering with intrusive elements. Figure 7 shows a nanofuel droplet in a disruptive process. The instant t = 0 ms is defined as the micro-explosion moment. This indicates that the primary droplet explodes, and its original shape is no longer spherical. However, prior to this event, the droplet distorts, and puffing is detected at t = -0.9375 ms. At this moment, no obvious fragments were released by the droplet. On the other hand, when the micro-explosion occurs, several fragments were released with smaller dimensions than the primary droplet, as shown at t = 0.3125 ms. As time proceeds, the number of fragments increases, and bright spots are identified as the aluminum combustion. From t = 0.625 ms to t = 0.9375 ms, the ignited fragments are dispersed in the quartz tube and appear to rotate in turn of the explosion position. During this process, the ignited fragments ascend, making their detection increasingly difficult (t = 1.5625 ms). Moreover, a major portion of the deformed droplet remains visible without significantly altering its position. The ignition of this part initiated at t = 5.625 ms, being noticeable at its surface brightness. In the course of time, an intense bright spot appears, which gradually extinguishes. Finally, a combustion residue is violently projected away, ending up ascending as the smoke tail. According to the literature, the micro-explosions are affected by the test temperature. Figure 8 shows the disruptive events occurred at T = 1000 °C. Before the micro-explosion (t = 0 ms), puffing is evident where at least two fragments are ejected. When the micro-explosion begins, a large number of ignited fragments are released in various directions, promoting intense bright spots inside the quartz tube. The ignited fragments rotate and ascend, possessing different dimensions. The largest fragment from the micro-explosion is divided into two elements, as displayed in t = 1.5 ms. As a result, another intense explosion occurs from t = 1.5 ms until t = 3.0 ms, leading to the appearance of more small fragments projected from the initial position. Subsequently, these fragments ignite and finally happen the total disintegration of the droplet.

Comparing the phenomena as a function of the furnace temperature, in terms of puffing and

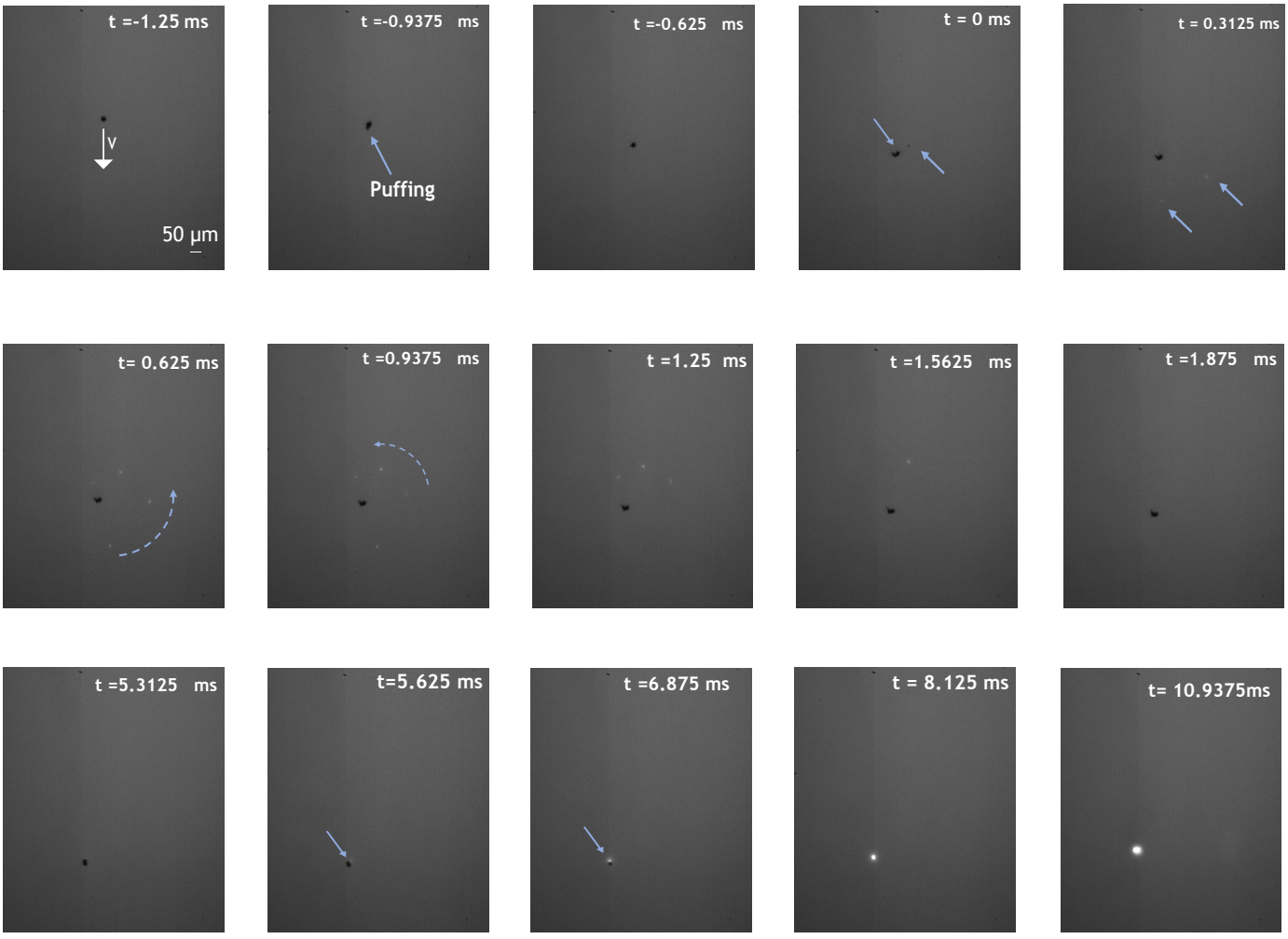

Figure 7. Disruptive burning phenomena at T = 800 °C, where t = 0 ms corresponds to the beginning of the micro-explosion.

micro-explosions, it was proved that both events occur for the operating conditions used in the present study. Nevertheless, the phenomena are more intense at T = 1000 °C, where the largest fragments disrupt into smaller fragments, leading to their ignition. At the lowest furnace temperature, a considerable portion of the droplet remains shapeless and, as time evolves, ignites as a single fragment. In this context, it is essential to evaluate the maximum number of fragments released from the micro-explosions. Figure 9 shows the maximum number of fragments after the micro-explosion occurrence at the two furnace temperatures. This empirical approach allows the investigation of the micro-explosion intensity based on the image data processing previously mentioned. The elements ejected by the puffing identified before the micro-explosion were not taken into account since they mostly are unnoticeable and scanty.

In addition, the fragments were only considered when their size was larger than the pixel size. As shown in Figure 9, a sample of 10 micro-explosions was examined and randomly sorted. The blue dashed line corresponds to the average value of fragments number at T = 800 °C and the red dashed line at T = 1000 °C, respectively. The presentation of these lines is merely to ease the

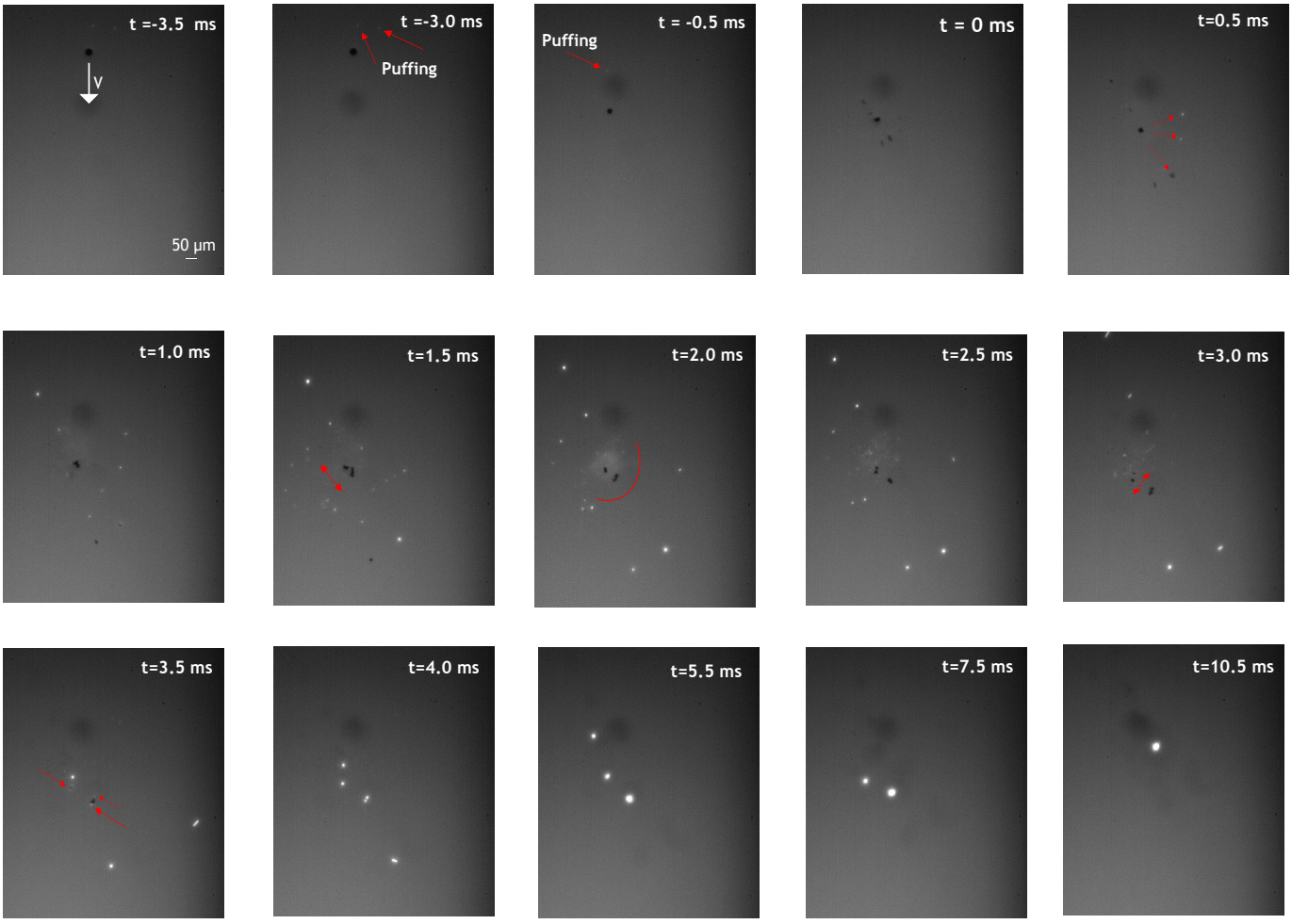

Figure 8. Disruptive burning phenomena at T = 1000 °C, where t = 0 ms corresponds to the beginning of the micro-explosion.

comprehension of data. The results indicate that the number of fragments is higher for the highest furnace temperature. As previously discussed, at T = 1000 °C, it was noticed that the largest fragments could break into additional elements with a reduced size leading to an effective dispersion. The dispersion of the particles greatly increases the surface area of the final agglomerates and consequently increases the air/fuel mixture of the solid phase fuel. Furthermore, at T = 800 °C, a large fragment burns individually without disrupting several elements after the explosion. This observation could be related to the increase of the furnace temperature allowing a quick accumulation of aluminum nanoparticles at the droplet surface, consequently increasing its temperature and promoting an intense explosion. To proceed with the micro-explosion study, Figure 10 shows a relation between the maximum number of fragments with the micro-explosion duration. A clear trend was challenging to notice due to unpredictability related to the phenomenon and the influence of temperature in the extinction of the fragments.

Each color point corresponds to a micro-explosions, where the red points correspond to T = 1000 °C

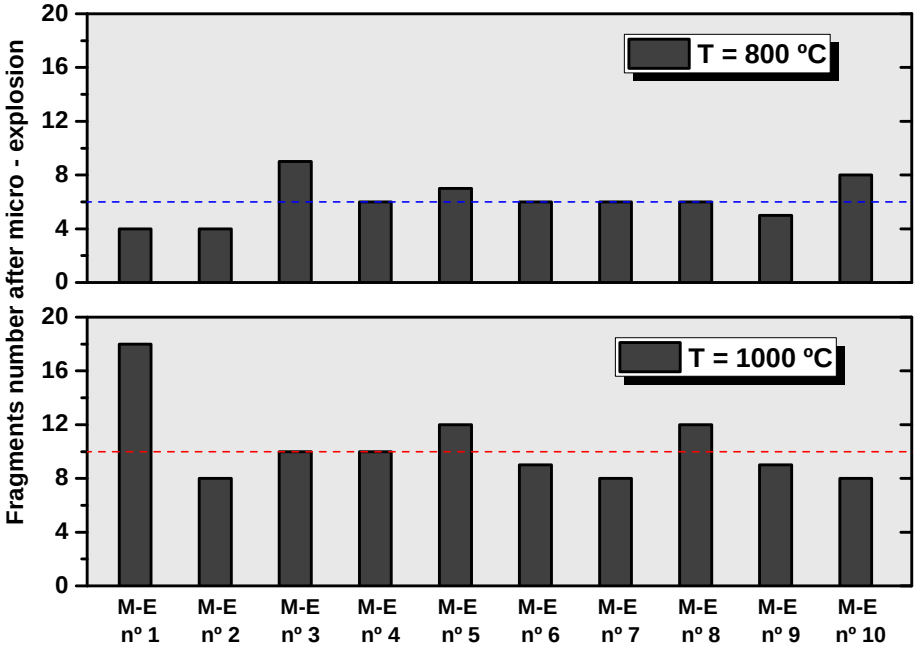

Figure 9. Number of fragments as a quantification method for micro-explosion (M-E) intensity.

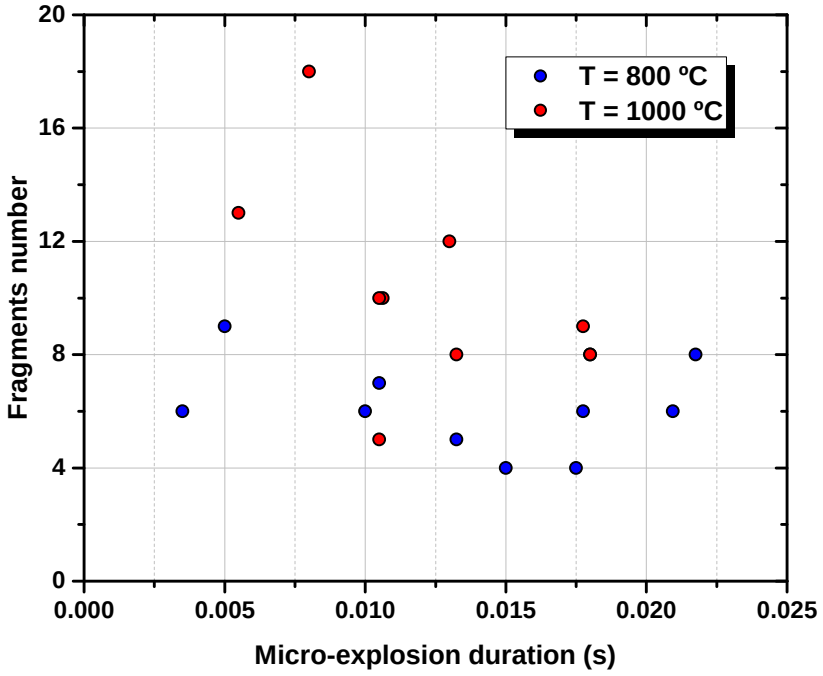

Figure 10. A relation between the number of fragments with the micro-explosion (M-E) duration.

and blue points correspond to T = 800 °C. The majority of micro-explosions occurred from approximately 0.010 s to 0.020 s. The highest fragment number released by the micro-explosions seems to possess a shorter duration. However, more studies should be performed to increase the study sample. It is essential to mention that 20 micro-explosions were considered due to the limitation in the field of view and the micro-explosion tracking.

In a falling droplet method, the convective environment and the flame position could be relevant factors that potentially influence the micro-explosions events. In light of this, Figure 11 shows the number of fragments at each region of interest for the test temperatures. The red circle represents the explosion position, and based on this 4 regions (upper side - right and left; lower side - right and left) were delimited with a maximum length of 500 pixels. Thus, the upper side has an opposite direction to the downward movement of the droplet. The lower side is in accordance with the droplet motion. First, it is important to highlight that the number of fragments presented in Figure 11 corresponded only one instant after the micro-explosions when the fragments were spotted. Due to this, and contrary to what has been explained above, the number of fragments for T = 800 °C seems to be higher. This observation is due to the identification of fragments right after the micro-explosions, and as noticed in Figure 8, as the time proceeds for a higher furnace temperature, the largest fragments tend to disrupt, producing more fragments with reduced time. A total of 60 fragments were considered, and different colors represent the results for the furnace temperature.

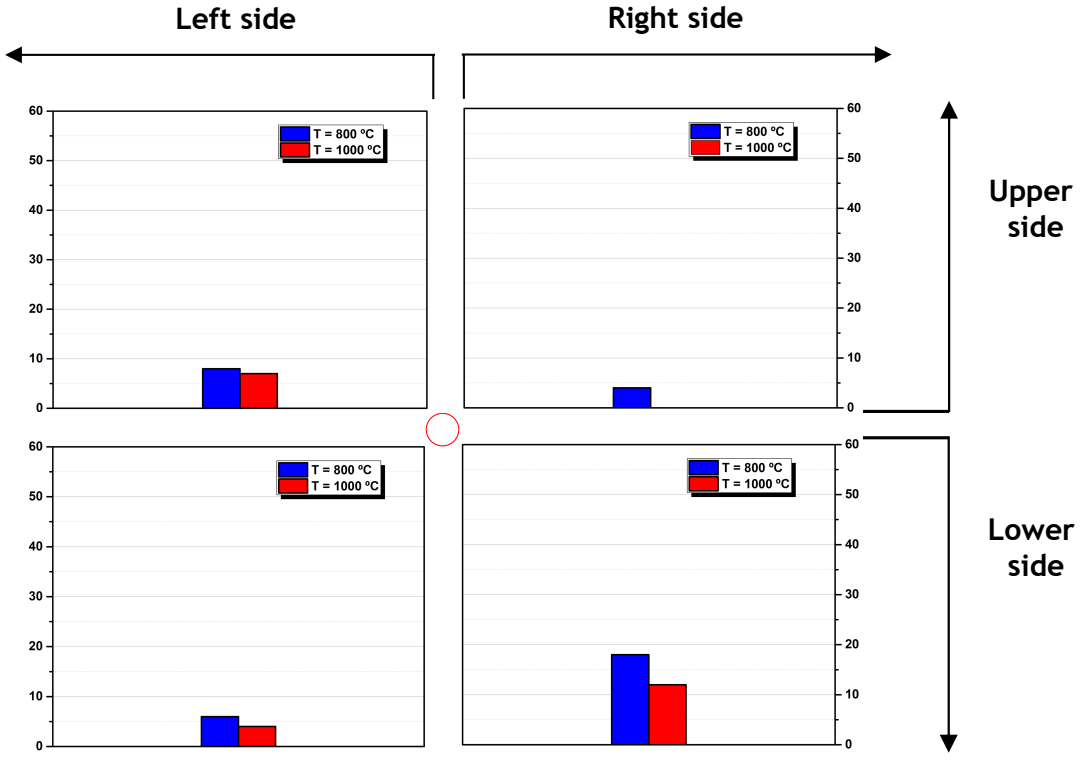

Figure 11. Number of fragments at each region of interest after the micro-explosion.

The results suggest that neither side has a considerable number of fragments to distinguish. How-

ever, the lower side possesses a higher number of fragments. Therefore, it was noticed that apparently, the droplet flame position does not affect the disruptive event. At the moment of a micro-explosion, the droplet flames is already extinguished, being easily identified in the upper side. Future studies on the dynamics within the droplet should be carried out to obtain more insights into the micro-explosions.

4. Conclusions

The present work experimentally evaluated the disruptive burning phenomena on nanofuel droplets. The combustion of pure HVO and nanofuel was compared in terms of burning rate and disruptive outcomes. It was concluded that adding aluminum combustion in a proper particle concentration can potentially improve the biofuel combustion performance. Moreover, no puffing or micro-explosions were detected in the pure HVO. In contrast, nanofuels displayed puffing and micro-explosions at the end of the droplet lifetime. In addition, the furnace temperature affects the disruptive process, being more intense at T = 1000 °C. It was observed that a higher number of fragments are ejected at the highest furnace temperature. In addition, the fragments after the explosion are mainly on the lower side, however more studies focused on this topic should be performed since these disruptive events are unpredictable. The image data acquisition provided the visualization and description of micro-explosions in nanofuel droplets, as well as comprehension of its phenomenology.

Acknowledgements

Inês A. S. Ferrão acknowledges Fundação para a Ciência e Tecnologia (FCT) for the provision of Ph.D scholarship with the reference SFRH/BD/144688/2019. The present work was performed under the scope of the Laboratório Associado em Energia, Transportes e Aeronáutica (LAETA) and Laboratório de Robótica e Sistemas de Engenharia (LARSyS) activities and it was supported by FCT through the projects number UIDB/50022/2020 and UIDB/50009/2020. Authors would also like to acknowledge Fundação para a Ciência e Tecnologia for partially supporting this work through project PTDC/EME-SIS/2017.

Nomenclature

DTF Drop tube furnace
HVO Hydrotreated vegetable oil
$M\text{-}E$ Micro-explosion
$n\text{-}Al$ Aluminum nanoparticles

References

Basu, S., & Miglani, A. (2016). Combustion and heat transfer characteristics of nanofluid fuel droplets: A short review. *International Journal of Heat and Mass Transfer*, *96*, 482–503.

Brenn, G., Deviprasath, L., Durst, F., & Fink, C. (2007). Evaporation of acoustically levitated multi-component liquid droplets. *International journal of heat and mass transfer*, *50*(25-26), 5073–5086.

Chung, S. S., & Kawaguchi, O. (1990). An experimental study on the evaporation of freely falling droplet under high temperature and high pressure gas stream. *KSME Journal*, *4*(2), 172–177.

Doliente, S. S., Narayan, A., Tapia, J. F. D., Samsatli, N. J., Zhao, Y., & Samsatli, S. (2020). Bio-aviation fuel: A comprehensive review and analysis of the supply chain components. *Frontiers in Energy Research*, *8*, 110.

Ferrão, I. A., Mendes, M. A., Moita, A. S., & Silva, A. R. (2022). The addition of particles to an alternative jet fuel. *Fuels*, *3*(2), 184–206.

Ferrão, I. A., Silva, A. R., Moita, A. S., Mendes, M. A., & Costa, M. M. (2021). Combustion characteristics of a single droplet of hydroprocessed vegetable oil blended with aluminum nanoparticles in a drop tube furnace. *Fuel*, *302*, 121160.

Gan, Y., & Qiao, L. (2011). Combustion characteristics of fuel droplets with addition of nano and micron-sized aluminum particles. *Combustion and Flame*, *158*(2), 354–368.

Gür, T. M. (2018). Review of electrical energy storage technologies, materials and systems: challenges and prospects for large-scale grid storage. *Energy & Environmental Science*, *11*(10), 2696–2767.

Hari, T. K., Yaakob, Z., & Binitha, N. N. (2015). Aviation biofuel from renewable resources: Routes, opportunities and challenges. *Renewable and Sustainable Energy Reviews*, *42*, 1234–1244.

Ittoo, B., Ooi, J. B., Tran, M.-V., Jaliliantabar, F., Najafi, G. H., & Swamy, V. (2022). Effects of dispersed multiwalled carbon nanotubes on the micro-explosion and combustion characteristics of 2-methylfuran–diesel mixture droplets. *Fuel*, *316*, 123308.

Jang, G. M., & Kim, N. I. (2022). Investigation on breakup characteristics of multicomponent single droplets of nanofluid and water-in-oil emulsion using a pulse laser. *Fuel*, *310*, 122300.

Javed, I., Baek, S. W., & Waheed, K. (2014). Effects of dense concentrations of aluminum nanoparticles on the evaporation behavior of kerosene droplet at elevated temperatures: The phenomenon of microexplosion. *Experimental thermal and fluid science*, *56*, 33–44.

Li, H., Pokhrel, S., Schowalter, M., Rosenauer, A., Kiefer, J., & Mädler, L. (2020). The gas-phase formation of tin dioxide nanoparticles in single droplet combustion and flame spray pyrolysis. *Combustion and flame*, *215*, 389–400.

Liu, Y. C., Savas, A. J., & Avedisian, C. T. (2013). The spherically symmetric droplet burning characteristics of jet-a and biofuels derived from camelina and tallow. *Fuel*, *108*, 824–832.

Meng, K., Bao, L., Li, F., Wang, C., & Lin, Q. (2021). Experimental understanding on combustion and micro-explosion characteristics of mixed droplets of aviation fuel, biodiesel and ethanol. *Journal of the Energy Institute*, *97*, 169–179.

Muelas, Á., Remacha, P., Martínez, A., & Ballester, J. (2017). Combustion behavior of jet a droplets and its blends with butanol. In *Turbo expo: Power for land, sea, and air* (Vol. 50848, p. V04AT04A073).

Nylund, N.-O., Erkkilä, K., Ahtiainen, M., Murtonen, T., Saikkonen, P., Amberla, A., & Aatola, H. (2011). Optimized usage of nexbtl renewable diesel fuel. *OPTIBIO. Espoo*.

Pacheco, G., Silva, A., & Costa, M. (2021). Single-droplet combustion of jet a-1, hydroprocessed vegetable oil, and their blends in a drop-tube furnace. *Energy & Fuels*, *35*(9), 7232–7241.

Parag, S., & Raghavan, V. (2009). Experimental investigation of burning rates of pure ethanol and ethanol blended fuels. *Combustion and Flame*, *156*(5), 997–1005.

Pizziol, B., Costa, M., Panão, M. O., & Silva, A. (2018). Multiple impinging jet air-assisted atomization. *Experimental Thermal and Fluid Science*, *96*, 303–310.

Prakash, A., & Davies, J. (2020). An investigation into the feasibility of alternative aviation fuels. In *Aiaa scitech 2020 forum* (p. 0642).

Rao, D. C. K., Karmakar, S., & Som, S. (2017). Puffing and micro-explosion behavior in combustion of butanol/jet a-1 and acetone-butanol-ethanol (abe)/jet a-1 fuel droplets. *Combustion Science and Technology*, *189*(10), 1796–1812.

Sim, H. S., Plascencia, M. A., Vargas, A., Bennewitz, J. W., Smith, O. I., & Karagozian, A. R. (2018). Effects of inert and energetic nanoparticles on burning liquid ethanol droplets. *Combustion Science and Technology*.

Singh, G., Esmaeilpour, M., & Ratner, A. (2019). The effect of acetylene black on droplet combustion and flame regime of petrodiesel and soy biodiesel. *Fuel*, *246*, 108–116.

Wang, J., Huang, X., Qiao, X., Ju, D., & Sun, C. (2020). Experimental study on effect of support fiber on fuel droplet vaporization at high temperatures. *Fuel*, *268*, 117407.

Wang, Z., Yuan, B., Huang, Y., Cao, J., Wang, Y., & Cheng, X. (2022). Progress in experimental investigations on evaporation characteristics of a fuel droplet. *Fuel Processing Technology*, *231*, 107243.

Yadav, A., Chowdhury, A., & Srivastava, A. (2021). Gas-phase thermography of droplet combustion and its application to characterize nanofuels. *International Communications in Heat and Mass Transfer*, *120*, 105054.